

Influence of process parameters in tungsten inert gas welding of titanium supported by you only look once – based defect detection algorithm

Przemysław Frankiewicz¹, Tomasz Góral¹, Michał Bembenek^{1*} 

¹ Faculty of Mechanical Engineering and Robotics, AGH University of Krakow, A. Mickiewicza 30, 30-059 Krakow, Poland

* Corresponding author's e-mail: bembenek@agh.edu.pl

ABSTRACT

Welding titanium remains a significant challenge because of its high reactivity with atmospheric gases at elevated temperatures, leading to potential defects. This study investigates the effect of welding parameters in tungsten inert gas (TIG) welding on the quality of titanium welds. Experimental trials were conducted on Grade 2 titanium sheets, varying key process factors such as current, shielding gas flow, and nozzle geometry. Additionally, artificial intelligence-based defect detection model using the YOLO convolutional neural network was applied to evaluate the weld quality. The results demonstrate that optimizing these parameters significantly reduces oxidation and improves weld penetration. The highest-quality weld was obtained using a welding current of 83 A, a shielding gas flow rate of 15 L/min at the weld face, 14 L/min from an auxiliary device, and 3 L/min at the weld root. A 14 mm nozzle with a gas lens effectively minimized surface oxidation, leading to a defect-free weld as confirmed by AI-based detection. The YOLO-based defect detection model achieved high precision and recall for most defect classes, including non-conformance (95.1% / 80.0%), geometric (87.8% / 71.4%), and post-processing defects (100% / 72.1%), with lower performance observed for adjacent (74.8% / 60.5%) and integrity defects (86.4% / 27.3%). This study confirms the potential of integrating AI into welding process evaluation, highlighting the role of shielding gas distribution in achieving high-quality titanium welds.

Keywords: titanium welding, TIG welding, weld quality, welding defect detection, artificial intelligence, YOLO algorithm.

INTRODUCTION

Titanium and its alloys, due to their exceptional mechanical, physical [1], and chemical properties [2], are key materials in the aerospace [3, 4], defense [5, 6], lightweight construction [7, 8], medical [9], and space technology industries [10]. They exhibit a high strength-to-weight ratio [11], excellent corrosion resistance, and the ability to operate in extreme conditions [12, 13]. The high cost of this metal also contributes to the perception that titanium applications are limited to industries and products with high-quality requirements [14, 15]. The global demand for titanium materials is expected to increase by 34% between 2025 and 2035 [16]. However, welding

titanium remains a technological challenge [17, 18], primarily due to its high affinity for atmospheric gases such as oxygen, nitrogen, and hydrogen, which, at elevated temperatures, lead to material embrittlement and a deterioration of its mechanical properties [19, 20]. The belief that titanium is difficult to weld likely stems from its physical [21] and chemical characteristics [22, 23], including its higher melting point compared to other metals and alloys [24], as well as the necessary precautions to prevent contamination during welding and protective layers to avoid oxidation [25]. Experience in titanium welding indicates that welding techniques for titanium and its alloys are very similar to those used for nickel alloys [26] and stainless steels, which improves

the perception of its weldability [27, 28]. Tungsten inert gas (TIG) welding is one of the most commonly used techniques for joining titanium and its alloys [29, 30]. This method allows for the production of high-quality welds [31], provided that process parameters are precisely controlled [32, 33]. Their optimization can significantly improve the microstructure and mechanical properties of welds [34], which is particularly important in industrial applications [35, 36]. The dynamic development of artificial intelligence-based technologies opens new possibilities in monitoring and evaluating weld quality [37, 38]. Systems based on deep neural networks enable rapid and precise detection of welding defects [39]. The introduction of such tools into production processes allows for automation and acceleration of weld quality assessment while reducing the risk of human errors [40, 41]. Despite progress in titanium welding, the literature indicates a shortage of studies combining TIG welding parameter optimization with modern machine learning systems for weld quality assessment [42, 43]. The objective of this study is to analyze the impact of TIG welding parameters on the quality of titanium welds, considering factors such as welding current, shielding gas flow, and nozzle geometry. Additionally, the feasibility of using the YOLO convolutional neural network for welding defect detection was evaluated, contributing to the development of effective tools supporting quality control in the industry.

METHODOLOGY

The first step in the research process was the acquisition of materials. The availability of titanium on the Polish market is limited, as it is not commonly found in metal suppliers specializing in non-ferrous metals. For this reason, commercially available Grade 2 titanium sheets with a thickness of 3 mm and dimensions of 100 × 300 mm were purchased for the study. This material is characterized by an excellent balance between strength and ductility while maintaining a low level of impurities. As part of the preparation, the chemical composition of the purchased titanium sheets was analyzed. The material properties are presented in Table 1.

To prevent heat-induced degradation of mechanical properties, the titanium sheets were cut into 42 × 100 mm test samples using a guillotine shear. This method minimized the risk of thermal damage during processing. In addition, TIG welding rods were required as filler material for the welding process. Prior to welding, specific procedures were followed to ensure the integrity of the process and the quality of the welds:

- Cleaning the groove and surrounding base material with a 30 mm diameter stainless steel brush on both sides of the weld seam.
- Using new and clean welding gloves and protective equipment.
- Inspecting the welding machine, power cables, and gas supply hoses.

Table 1. Material certification of Grade 2 titanium sheets. [44]

Chemical composition		
Chemical element	Requirement [%]	Content [%]
Fe	< 0.2	0.028
C	< 0.06	0.0085
N	< 0.05	0.003
H	< 0.013	0.00085
O	< 0.16	0.14
Basic mechanical properties		
Material property	Requirement [MPa]	Result [MPa]
Tensile strength	390–540	433–451
Yield strength 1%	> 270	336–338
Yield strength 0.2%	> 250	302–316
Other mechanical properties		
Material property	Requirement [-]	Result [-]
Elongation	> 22 [%]	30 [%]
Hardness (HRB)	< 100	84.6

- Cleaning the tungsten electrode tip before starting the welding process, and properly introducing the filler material into the weld pool during welding. Ensuring shielding gas protection by maintaining a 25-second gas flow before and after welding, allowing the weld temperature to drop below 300 °C.

The experiments were conducted using an inverter-based welding power source, Kemppi MasterTig MLS 2300ACDC. To ensure proper shielding, a gas protection system was used, providing a stable argon flow to both the front and back sides of the weld.

The study involved six different sets of welding parameters to assess their influence on weld quality. The analyzed factors included:

- Welding current. The current was set in two stages: initial and continuous. This approach allowed for controlled material preheating and ensured process stability. The tested current values ranged from 70A to 85A for the initial phase and from 60 A to 83 A for the continuous phase. Higher currents aimed to improve weld penetration, while lower currents were used to minimize overheating and oxidation risks.
- Shielding gas flow. The shielding gas flow rate was varied for both the front (face) and back (root) of the weld, ranging from 2 L/min to 16.5 L/min. Industrial-grade high-purity argon (99.999%) was used to protect

the weld from atmospheric contamination, such as oxygen, nitrogen, and hydrogen, which could degrade mechanical properties [45]. Higher gas flow rates were applied to the weld face to ensure a uniform surface, whereas lower flow rates on the weld root helped reduce gas loss [46, 47].

- Nozzle geometry and type. Two types of welding nozzles were tested: 14 mm and 20 mm in diameter, with and without gas lenses. The use of gas lenses aimed to improve the distribution of shielding gas, thereby reducing oxidation and enhancing weld uniformity [48].
- Additional shielding gas supply. In some experiments, additional gas supply devices were used to increase shielding gas flow on the weld face. These devices were implemented to minimize common defects, such as porosity and oxidation, which can occur under challenging welding conditions.

The specific nozzles and auxiliary gas devices used in this study are presented in Figure 1 and Figure 2.

Each of the six welding parameter sets was designed to allow for:

- The evaluation of weld penetration based on varying current values.
- The analysis of weld face and root surface quality, focusing on uniformity and defect presence.

(A)



(B)



Figure 1. The 14 mm nozzle with a gas lens (A) and the 20 mm nozzle without a gas lens (B)

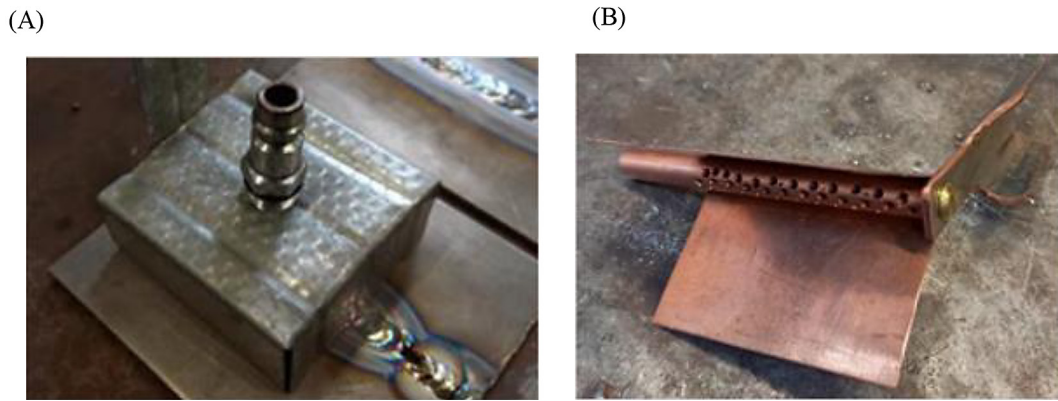


Figure 2. Two types of the auxiliary shielding gas devices (A) and (B)

- The examination of nozzle geometry impact on gas distribution and its effect on weld surface quality.

To assist in the visual analysis of titanium weld quality obtained using the TIG method, a YOLO (you only look once) convolutional neural network was implemented [49]. The purpose of this approach was to enable automatic detection and classification of welding defects based on image analysis, which significantly accelerated the evaluation process and reduced subjective errors associated with human inspection. The YOLO network was trained using a customized dataset consisting of photographic images of welds captured with conventional cameras. This dataset was specifically adapted for weld defect detection and was sourced from a publicly available dataset on the Kaggle platform. The dataset used in the analysis was designed for detecting welding defects in conventional images, excluding HDR, radiographic, or X-ray images. The dataset consists of annotated images formatted for YOLO training and includes the following weld defect categories: adjacent defects, such as spatter and arc marks; integrity defects, including porosity, cracks, and inclusions; geometric defects, such as undercuts and lack of fusion; post-processing defects, including scratches and

burrs; and non-conformance defects, specifically lack of fusion and incomplete penetration. The data was divided into three subsets: the training set (85%), used for model training; the validation set (10%), used to evaluate model performance during training; and the test set (5%), used for final assessment on previously unseen data. The distribution of annotated weld defects within each subset was unevenly spread across defect categories, reflecting their natural frequency of occurrence in welding processes. Common defects, such as spatter or surface irregularities, appeared more frequently, whereas critical defects, such as lack of penetration, were less common. Table 2 presents the detailed distribution of defects in the training and validation datasets. Despite the uneven distribution of defect categories, this dataset was accepted for training, as frequently occurring defects, such as spatter, are representative of most welding processes, while rarer defects, such as lack of penetration, are easier to detect at earlier welding stages. The YOLO model was designed to account for this imbalance, assigning higher weights to rare but critical defects to improve detection accuracy [50, 51].

The number of detected defects alone is not sufficient for a comprehensive evaluation of weld acceptability, as each defect class has a different impact on the structural integrity of the welded

Table 2. Distribution of defects in the training and validation sets

Defect class	Training Set	Validation Set
Adjacent defects: spatter, arc marks (adj)	1278	238
Integrity defects: porosity, cracks, inclusions (int)	657	124
Geometric defects: undercuts, lack of Fusion (geo)	855	160
Post-processing defects: scratches, burrs (pro)	225	46
Non-conformance defects: lack of fusion, incomplete penetration (non)	161	34

joint. Therefore, an acceptability index (WA) was introduced, which considers not only the number of detected defects but also their severity, size, and technical significance. This approach allows for an objective and consistent assessment of results, particularly in cases where defect classes are unevenly distributed in the dataset (Table 3).

The WA index is defined by Equation 1, where each defect class is assigned a specific weight that reflects its significance for the integrity of the weld:

$$WA = \sum_{i=1}^n Class\ weight_i \times Defect\ count_i \times Size\ modifier_i \quad (1)$$

where: *Class weight* – a coefficient assigned to each defect class, indicating its impact on weld integrity, *Defect count* – the number of defects detected for a given class, *Size modifier* – a coefficient that considers the size of the bounding box in relation to the overall image area.

The weights were assigned based on the impact of each defect type on weld integrity. For example, defects in the non-conformance (non) category, such as incomplete penetration, can significantly weaken the weld, whereas post-processing (pro) defects, like scratches or burrs, have primarily cosmetic effects and do not compromise structural integrity.

To further account for defect size, a bounding box size modifier was introduced:

- Size modifier = 1.5 if the bounding box covers more than 2% of the total image area,
- Size modifier = 1.0 if the bounding box covers less than 2% of the total image area.

This coefficient helps to highlight large defects that may have a greater impact on the overall integrity of the weld, as opposed to small surface irregularities. A threshold criterion was established to define whether a weld is acceptable. If the acceptability index $WA \geq 5$, the weld is considered unacceptable, meaning it contains

too many or too severe defects. This approach allows not only for the identification of samples with the highest number of defects but also for their assessment based on their impact on mechanical strength and structural integrity. For example, a weld with multiple adjacent defects (adj) may still be deemed acceptable, whereas the presence of a single critical defect (non) would result in rejection.

RESULTS

In this study, the YOLOv5s model was trained on a dataset of welding seam images with precisely labeled defect classes. The dataset contained a diverse distribution of defect types, including adjacent, integrity, geometric, post-processing, and non-conformance defects. Figure 3 illustrates the distribution of defect classes in the training dataset, highlighting the imbalance in defect occurrence, which was accounted for during model training.

To evaluate the effectiveness of the model, YOLO-based defect detection was performed on test images, allowing for visual assessment of detected defects. The detection results were overlaid on sample weld images, where bounding boxes indicate the identified defects and their respective classifications. The effectiveness of the model in distinguishing between different defect types is presented in Figure 4.

The training process involved the following network parameters. All input images were resized to 640×640 pixels (imgsz) to ensure a consistent visual representation for the model. The training was conducted over 50 full iterations (epochs), allowing the model to gradually learn while minimizing the risk of overfitting. The batch size was set to 16 images per iteration, striking a balance between processing speed and the stability of weight updates. For optimization, the AdamW optimizer was employed [52], which dynamically adjusted the initial learning rate and momentum, enhancing training stability.

Table 3. Assigned weights for each defect class and their impact on weld acceptability

Defect class	Class weight	Technical significance
Adjacent defects (adj)	0.5	Minor defects, acceptable in most cases
Integrity defects (int)	3.0	Major defects that result in weld rejection
Geometric defects (geo)	2.0	Moderate defects that affect weld strength
Post-processing defects (pro)	0.2	Cosmetic defects, generally acceptable
Non-conformance defects (non)	4.0	Critical defects, always unacceptable

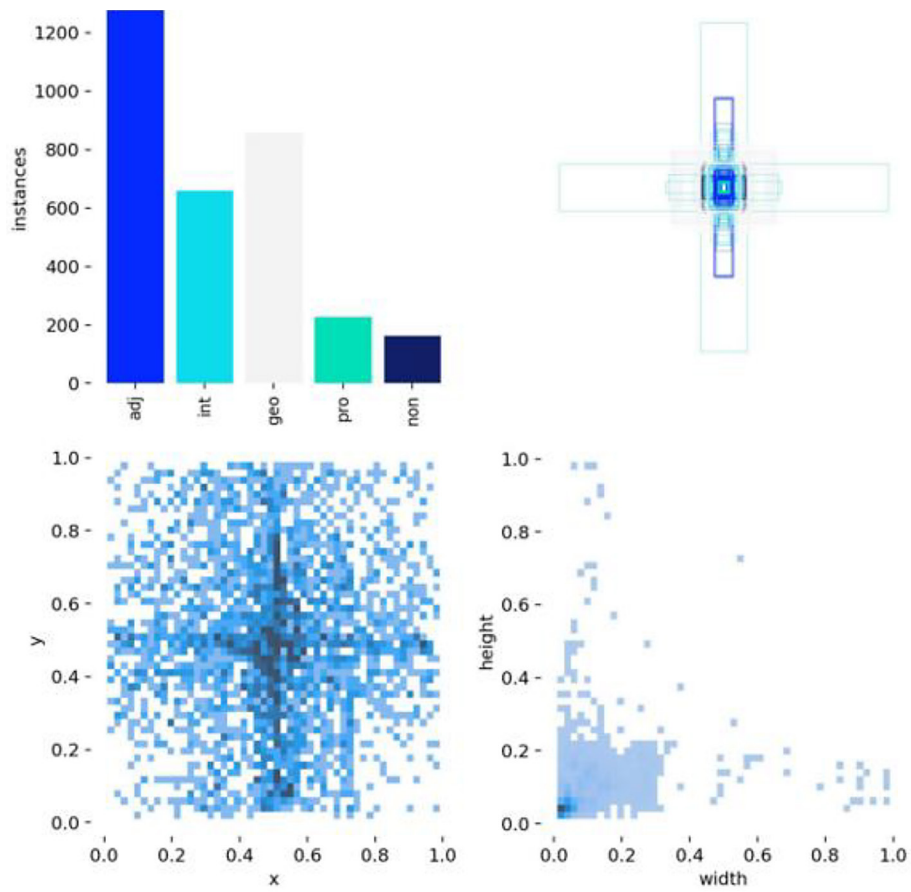


Figure 3. Uneven distribution of welding defects in the training dataset

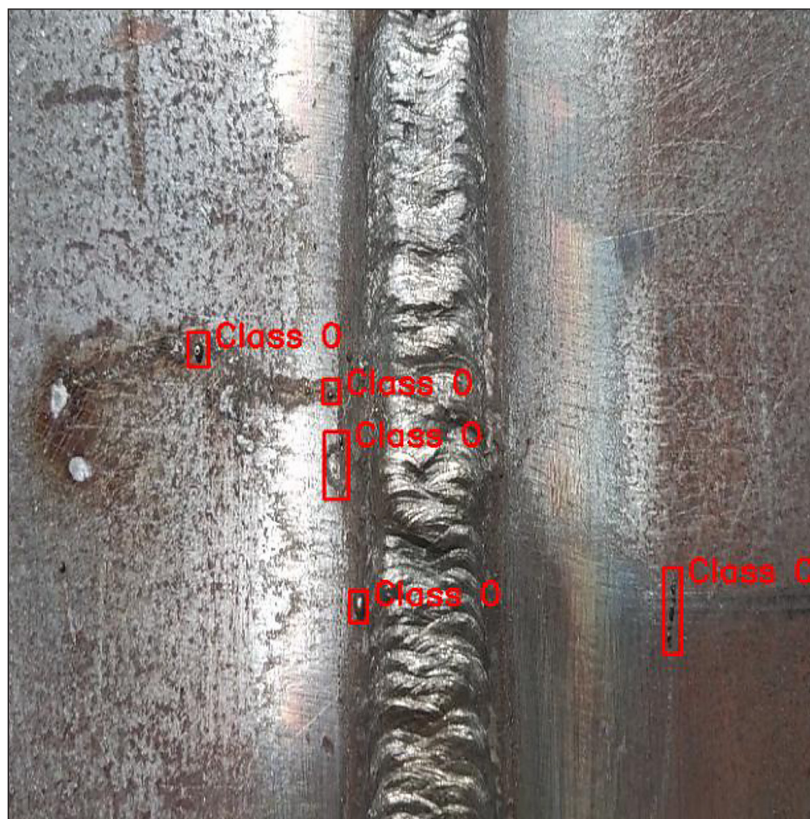


Figure 4. Example of weld defect detection using the YOLO model

Throughout the training process, loss function values were monitored in three categories:

- Box Loss indicates how well the predicted bounding boxes align with actual objects. The loss initially measured 4.27 and decreased to 1.81 after 50 epochs.
- Class Loss represents the accuracy of defect classification. Its value dropped from 5.71 to 1.39, indicating improved class assignments.
- DFL Loss (distribution focal loss) quantifies the precision of key point predictions for objects, reducing from 4.16 to 1.66 over the training period.

These loss function trends are illustrated in Figure 5. The loss values steadily declined over the course of successive training epochs. The initial values of 4.27 (Box Loss), 5.71 (Class Loss), and 4.16 (DFL Loss) underwent a significant reduction, reaching 1.81, 1.39, and 1.66, respectively, in the final training stages. The stable nature of these loss curves suggests that the model successfully adapted to the training dataset without signs of overfitting [53].

After completing the training phase, the model was validated on an independent test dataset. The results are presented in Table 4 and Figure 6.

The geo, non, and pro defect categories exhibit a broad area under the Precision-Recall curve, confirming their high detection accuracy. However, for the int and adj categories, steeper declines were observed, indicating that the model struggles to maintain high precision as recall increases. The classification performance metrics presented in Table 5 and the Precision-Recall curve demonstrate that the model is particularly effective at detecting geometric and post-processing defects, whereas the detection of adjacent and integrity defects requires further optimization.

After validating the YOLOv5 model, an analysis of test samples was conducted to evaluate the quality of welds produced under different technological parameters.

Test sample 1

For this sample, moderate welding parameters were applied. The initial current was set

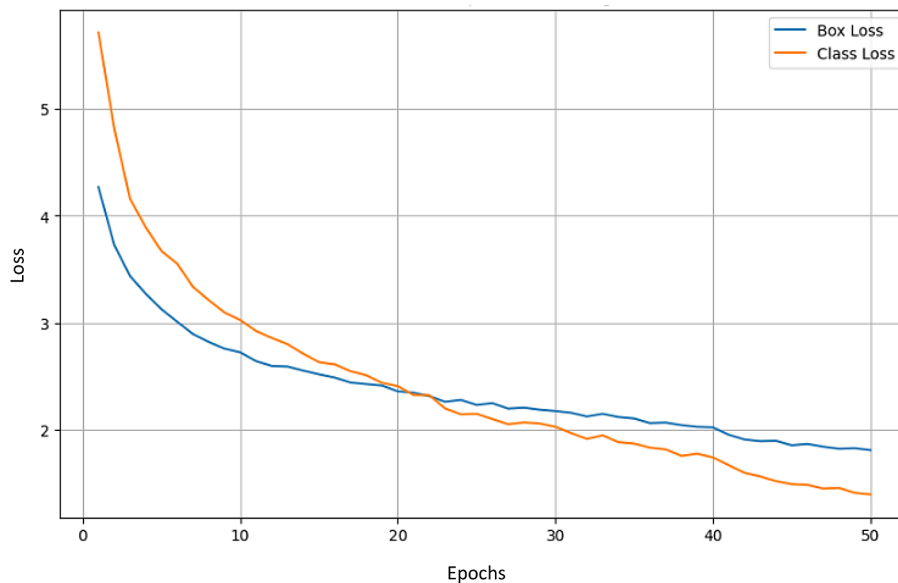


Figure 5. Loss function variations during training, where the Y-axis shows the dimensionless loss value, while the X-axis indicates the epoch number

Table 4. Classifier performance metrics

Defect class	Precision	Recall	mAP50	mAP50-95
Adjacent defects (adj)	0.747890	0.605263	0.680528	0.289413
Integrity defects (int)	0.863606	0.272727	0.379583	0.181580
Geometric defects (geo)	0.877534	0.714286	0.887691	0.519983
Post-processing defects (pro)	1.000000	0.720885	0.828551	0.305944
Non-conformance defects (non)	0.951027	0.800000	0.802355	0.454421

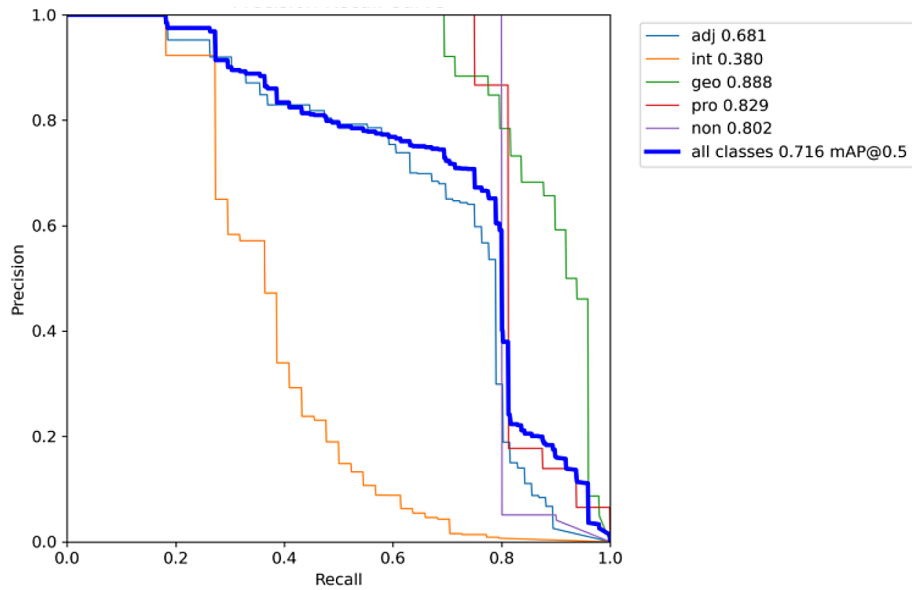


Figure 6. Precision-Recall curve

Table 5. Technological parameters for welding test sample 1

Test sample 1	Parameter value
Welding current	Initial – 70 A, continuous – 60 A
Shielding gas (weld face)	15 L/min
Shielding gas (weld root)	4 L/min
Nozzle type	ø14 mm with a gas lens
Additional shielding gas device	None

to 70 A, while the continuous current was maintained at 60 A. The shielding gas was supplied at a flow rate of 15 L/min for the weld face and 4 L/min for the weld root. The absence of additional shielding gas devices resulted in limited oxidation protection. However, the 14 mm diameter nozzle with a gas lens provided moderate protection for the weld face.

The YOLOv5 model did not detect any defects in this weld, and the sample was classified as acceptable. The results for this test sample are summarized in Table 5 and illustrated in Figure 7.

Test sample 2

For this test, higher welding parameters were applied. The initial current was set to 83A, while the continuous current was maintained at 75 A. The shielding gas flow rate was 16.5 L/min for the weld face and 2 L/min for the weld root. Additionally, an auxiliary shielding gas device was used, supplying an extra 6 L/min of gas to the weld face. A 20 mm diameter nozzle without a gas lens was used, which provided less oxidation protection compared to the previous test using a

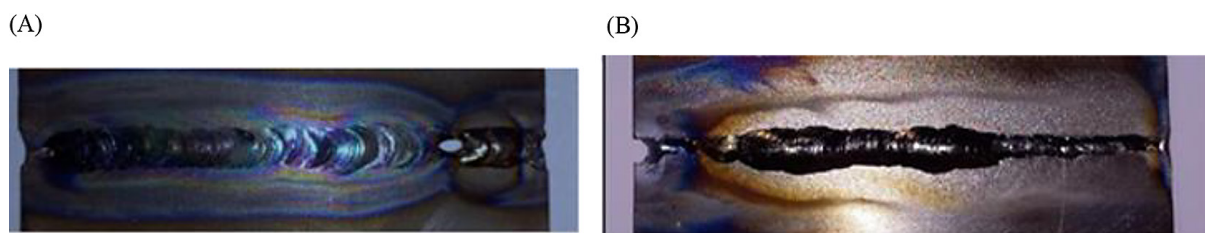


Figure 7. The test sample from the weld face (A) and weld root perspectives (B)

gas lens-equipped nozzle. However, the YOLOv5 model did not detect any defects, and the sample was classified as acceptable.

The results for this test sample are summarized in Table 6 and illustrated in Figure 8.

Test sample 3

For this test, the initial welding current was set to 80 A, while the continuous current was maintained at 70 A. The shielding gas flow rate was 15 L/min for the weld face and 4 L/min for the weld root. The absence of an auxiliary shielding gas device resulted in reduced oxidation protection, despite the use of a 14 mm diameter nozzle with a gas lens.

Nevertheless, the YOLOv5 model did not detect any defects, and the sample was classified as acceptable. The results for this test sample are summarized in Table 7 and illustrated in Figure 9.

Test sample 4

The welding parameters in this test were very similar to those used in test sample 2. The initial welding current was set to 83 A, while the continuous current remained at 75 A. The shielding gas flow rate was 16.5 L/min for the weld face and 2 L/min for the weld root, with an additional 10 L/min of shielding gas supplied by an auxiliary gas device.

Table 6. Technological parameters for welding test sample 2

Test sample 2	Parameter value
Welding current	Initial – 83 A, continuous – 75 A
Shielding gas (weld face)	16.5 L/min
Shielding gas (weld root)	2 L/min
Nozzle type	ø20 mm without a gas lens
Additional shielding gas device	6 L/min

Table 7. Technological parameters for welding test sample 3

Test sample 3	Parameter value
Welding current	Initial – 80 A, continuous – 70 A
Shielding gas (weld face)	15 L/min
Shielding gas (weld root)	2 L/min
Nozzle type	Ø14 mm with a gas lens
Additional shielding gas device	None

(A)



(B)



Figure 8. The test sample from the weld face (A) and weld root perspectives (B)

(A)



(B)



Figure 9. The test sample from the weld face (A) and weld root perspectives (B)

A 20 mm diameter nozzle without a gas lens was used. The YOLOv5 model did not detect any defects, confirming the acceptability of the weld. The results for this test sample are summarized in Table 8 and illustrated in Figure 10.

Test sample 5

Test sample 5 was identified as the most optimal configuration in terms of technological parameters. The welding process was conducted with a stable current of 83 A, a shielding gas flow rate of 15 L/min for the weld face, 3 L/min for the weld root, and an additional 14 L/min of shielding gas supplied by an auxiliary gas device. These conditions created ideal welding parameters, ensuring high-quality welds.

A 14 mm diameter nozzle with a gas lens was used, providing excellent oxidation protection. The YOLOv5 model confirmed that the weld was free of defects, classifying the sample as acceptable. The results for this test sample are summarized in Table 9 and illustrated in Figures 11.

Test sample 6

The final test was conducted with an initial welding current of 85 A, while the continuous current was maintained at 80 A. The shielding gas flow rate was 15 L/min for the weld face and 2 L/min for the weld root, with an additional 16 L/min of shielding gas supplied by an auxiliary gas device.

Table 8. Technological parameters for welding test sample 4

Test sample 4	Parameter value
Welding current	Initial – 83 A, continuous 75 A
Shielding gas (weld face)	16,5 L/min
Shielding gas (weld root)	2 L/min
Nozzle type	Ø20 mm without a gas lens
Additional shielding gas device	10 L/min

Table 9. Technological parameters for welding test sample 5

Test sample 5	Parameter value
Welding current	Initial – 83 A, continuous – 83 A
Shielding gas (weld face)	15 L/min
Shielding gas (weld root)	3 L/min
Nozzle type	Ø14 mm with a gas lens
Additional shielding gas device	14 L/min

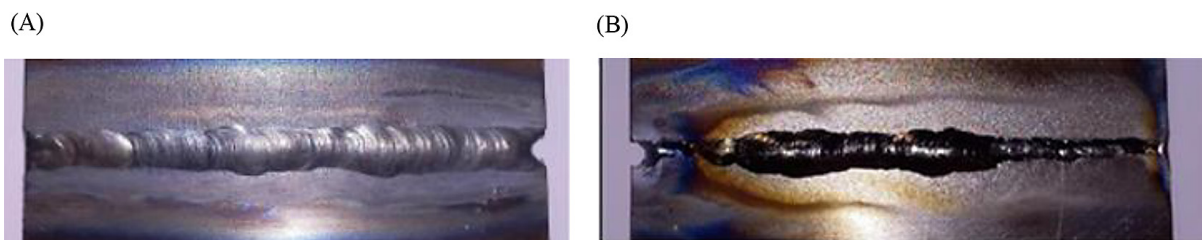


Figure 10. The test sample from the weld face (A) and weld root perspectives (B)

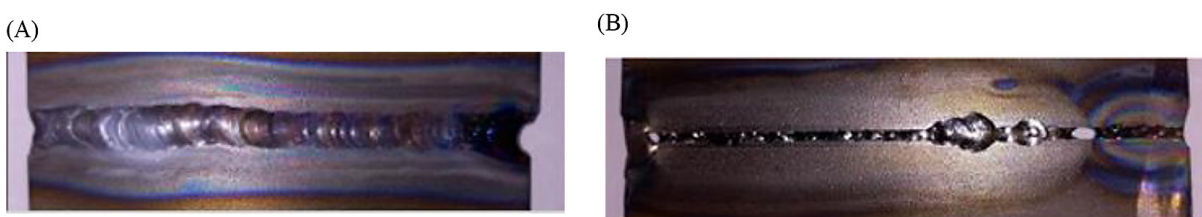


Figure 11. The test sample from the weld face (A) and weld root perspectives (B)

A 14 mm diameter nozzle with a gas lens was used, ensuring good oxidation protection. The YOLOv5 model did not detect any defects, and the sample was classified as acceptable. The results for this test sample are summarized in Tables 10, 11 and illustrated in Figure 12.

To provide a clear overview of all welding trials, a summary table has been added below, listing the technological parameters and classification outcomes for each test sample.

DISCUSSION

The weld samples were evaluated using expert visual inspection (VT2) supported by AI-based analysis [40]. The YOLOv5s model detected no defects, likely due to its limitation in identifying surface oxidation, which is a critical issue in

titanium welding but falls outside the model’s detection capabilities [42, 43]. Test sample 5 exhibited the best results due to an optimized shielding gas flow, a gas-lens-equipped nozzle, and a stable welding current, which collectively reduced defect occurrence. A key factor in its superior quality was minimized oxidation. The 14 mm gas-lens nozzle provided stable argon shielding, effectively displacing reactive atmospheric gases, while an auxiliary gas supply of 14 L/min further protected the heat-affected zone. Additionally, the welding current of 83 A ensured deep penetration and structural integrity without excessive heat input, avoiding grain growth and internal stresses. The controlled 3 L/min gas flow at the weld root prevented contamination from oxygen and nitrogen exposure. These findings emphasize the importance of precise shielding gas distribution in TIG welding to achieve defect-free titanium joints [35].

Table 10. Technological parameters for welding test sample 6

Test sample 6	Parameter value
Welding current	Initial – 85 A, continuous – 80 A
Shielding gas (weld face)	15 L/min
Shielding gas (weld root)	2 L/min
Nozzle type	Ø14 mm with a gas lens
Additional shielding gas device	16 L/min

Table 11. Summary of technological parameters for all welding test samples

Test sample	Initial current [A]	Continuous current [A]	Shielding gas (face) [L/min]	Shielding gas (root) [L/min]	Additional gas device [L/min]	Nozzle type	YOLOv5 classification
1	70	60	15	4	None	Ø14 mm with gas lens	Acceptable
2	83	75	16.5	2	6	Ø20 mm without gas lens	Acceptable
3	80	70	15	2	None	Ø14 mm with gas lens	Acceptable
4	83	75	16.5	2	10	Ø20 mm without gas lens	Acceptable
5	83	83	15	3	14	Ø14 mm with gas lens	Acceptable
6	85	80	15	2	16	Ø14 mm with gas lens	Acceptable

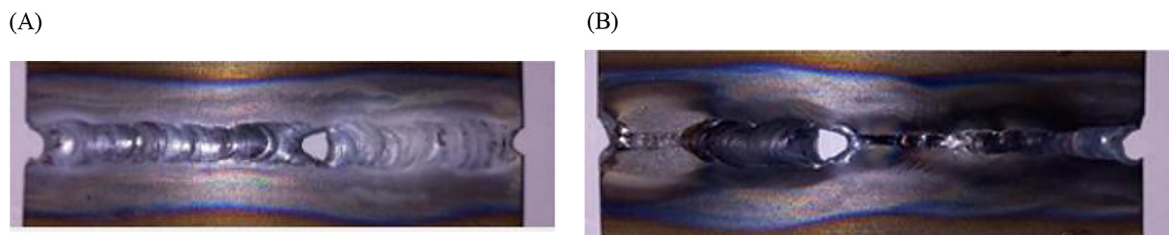


Figure 12. The test sample from the weld face (A) and weld root perspectives (B)

CONCLUSIONS

The conducted research demonstrated that the quality of titanium welds strongly depends on the precise selection of welding parameters and shielding gas technology. The best results were obtained in test sample 5, where the optimal conditions included a welding current of 83 A, a shielding gas flow rate of 15 L/min for the weld face, 14 L/min from the auxiliary gas device, and 3 L/min for the weld root, along with a gas-lens-equipped nozzle, which significantly reduced oxidation. The trained YOLOv5 model effectively assisted in visual weld inspection, particularly in identifying common defects, such as geometric irregularities. However, it struggled with the detection of rare defects affecting structural integrity. The absence of detected defects in certain samples might be related to the specific nature of titanium welds, where oxidation remains the primary concern. The results confirm that AI-based systems can enhance weld quality assessment, but human expertise and thorough visual inspection remain essential. The findings highlight the need for further advancements in shielding gas technologies and analytical algorithms to meet the challenges associated with welding titanium.

Acknowledgements

We would like to thank MSc Eng. Bartłomiej Duda for his contribution to the research work that supported this study.

Dataset

Sukma Adhi Wijaya (2021). Weld Defect Detection Dataset. Licensed under CC0 1.0 Universal. Available at: <https://www.kaggle.com/datasets/sukmaadhiwijaya/weld-defect-detection-dataset> 14.02.2025 12:10

REFERENCES

1. Saurabh A, Meghana CM, Singh PK, Verma PC. Titanium-based materials: synthesis, properties, and applications. *Materials Today: Proceedings*. 2022;56:412–9. <https://doi.org/10.1016/j.matpr.2022.01.268>
2. Tshephe TS, Akinwamide SO, Olevsky E, Olubambi PA. Additive manufacturing of titanium-based alloys- A review of methods, properties, challenges, and prospects. *Heliyon*. 2022;8(3):e09041. <https://doi.org/10.1016/j.heliyon.2022.e09041>.
3. Zhao Q, Sun Q, Xin S, Chen Y, Wu C, Wang H, et al. High-strength titanium alloys for aerospace engineering applications: A review on melting-forging process. *Materials Science and Engineering: A*. 2022;845:143260. <https://doi.org/10.1016/j.msea.2022.143260>
4. Williams JC, Boyer RR. Opportunities and issues in the application of titanium alloys for aerospace components. *Metals*. 2020;10(6):705. <https://doi.org/10.3390/met10060705>
5. Siengchin S. A review on lightweight materials for defence applications: Present and future developments. *Defence Technology*. 2023;24:1–17. <https://doi.org/10.1016/j.dt.2023.02.025>
6. Jiayong Z, Fanzhe M, Xiaopu W. Titanium alloy artillery barrel and radial precision forging technology discussion. *Journal of Physics: Conference Series*. 2023;2478(9):092034. <https://dx.doi.org/10.1088/1742-6596/2478/9/092034>
7. Jobanpreet S, Srivastawa K, Jana S, Dixit C, S R. Advancements in lightweight materials for aerospace structures: a comprehensive review. *Acceleration Aerospace Journal*. 2024;2(3):173–83. <https://doi.org/10.61359/11.2106-2409>
8. Hassan HZ, Saeed NM. Advancements and applications of lightweight structures: a comprehensive review. *Discover Civil Engineering*. 2024;1(1). <https://doi.org/10.1007/s44290-024-00049-z>
9. Marin E, Lanzutti A. Biomedical applications of titanium alloys: a comprehensive review. *Materials*. 2024;17(1):114. <https://doi.org/10.3390/ma17010114>
10. Pushp P, Dasharath SM, Arati C. Classification and applications of titanium and its alloys. *Materials Today: Proceedings*. 2022;54:537–42. <https://doi.org/10.1016/j.matpr.2022.01.008>
11. Blanco D, Rubio EM, Lorente-Pedreille RM, Sáenz-Nuño MA. Sustainable processes in aluminium, magnesium, and titanium alloys applied to the transport sector: a review. *Metals*. 2022;12(1):9. <https://doi.org/10.3390/met12010009>
12. Tolvanen S, Pederson R, Klement U. Microstructure and mechanical properties of Ti-6Al-4V welds produced with different processes. *Materials*. 2024;17(4):782. <https://doi.org/10.3390/ma17040782>
13. Najafizadeh M, Yazdi S, Bozorg M, Ghasempour-Mouziraji M, Hosseinzadeh M, Zarrabian M, et al. Classification and applications of titanium and its alloys: A review. *Journal of Alloys and Compounds Communications*. 2024;3:100019. <https://doi.org/10.1016/j.jacomc.2024.100019>
14. Sanjay M R, Doddamani S, Siengchin S, Doddamani

- M. Lightweight and Sustainable Composite Materials: Preparation, Properties and Applications 2023.
15. Chumaevskii A, Amirov A, Ivanov A, Rubtsov V, Kolubaev E. Friction stir welding/processing of various metals with working tools of different materials and its peculiarities for titanium alloys: a review. *Metals*. 2023;13(5):970. <https://doi.org/10.3390/met13050970>
 16. Polmear I, StJohn D, Nie JF, Qian M. Light alloys : metallurgy of the light metals 2017.
 17. Bodunrin MO, Chown LH, Omotoyinbo JA. Development of low-cost titanium alloys: A chronicle of challenges and opportunities. *Materials Today: Proceedings*. 2021;38:564–9. <https://doi.org/10.1016/j.matpr.2020.02.978>
 18. Zdrodowska K, WK, Szala M. The microstructural properties of explosion welded Ni/Ti joint. *Advances in Science and Technology Research Journal*. 2014;8(22):71–4.
 19. Bendikiene R, Baskutis S, Baskutiene J, Ciuplys A, Kacinskas T. Comparative study of TIG welded commercially pure titanium. *Journal of Manufacturing Processes*. 2018;36:155–63. <https://doi.org/10.1016/j.jmapro.2018.10.007>
 20. Peters M, Hemptenmacher J, Kumpfert J, Leyens C. Structure and properties of titanium and titanium alloys. *Titanium and Titanium Alloys* 2003;1–36. <https://doi.org/10.1002/3527602119.ch1>
 21. Balasubramanian TS, Balakrishnan M, Balasubramanian V, Muthu Manickam M. Effect of welding processes on joint characteristics of Ti–6Al–4V alloy. *Science and Technology of Welding and Joining*. 2011;16(8):702–8. <https://doi.org/10.1179/1362171811y.00000000062>
 22. Cui S-w, Shi Y-h, Zhang C-s. Microstructure and mechanical properties of TC4 titanium alloy K-TIG welded joints. *Transactions of Nonferrous Metals Society of China*. 2021;31(2):416–25. [https://doi.org/10.1016/S1003-6326\(21\)65506-1](https://doi.org/10.1016/S1003-6326(21)65506-1)
 23. Karpagaraj A, Siva shanmugam N, Sankaranarayanan K. Some studies on mechanical properties and microstructural characterization of automated TIG welding of thin commercially pure titanium sheets. *Materials Science and Engineering: A*. 2015;640:180–9. <https://doi.org/10.1016/j.msea.2015.05.056>
 24. Ghosh PS, Sen A, Chattopadhyaya S, Sharma S, Singh J, Li C, et al. Progressive developments and challenges in dissimilar laser welding of steel to various other light alloys (Al/Ti/Mg): A comprehensive review. *Heliyon*. 2022;8(11):e11710. <https://dx.doi.org/10.1016/j.heliyon.2022.e11710>
 25. Dewangan S, Ranjan R, Chattopadhyaya S, Gope D, Bogdan-Chudy M. Preliminary investigations of structure and properties of TIG Welded Ti-6Al-4V alloy. *Advances in Science and Technology Research Journal*. 2021;15(1):156–65. <https://dx.doi.org/10.12913/22998624/131064>
 26. Pawlik J, Bembenek M, Góral T, Cieřlik J, Krawczyk J, Łukaszek-Sołek A, et al. On the influence of heat input on Ni-WC GMAW hardfaced coating properties. *Materials*. 2023;16(11):3960. <https://doi.org/10.3390/ma16113960>
 27. Rominiyi AL, Mashinini PM. A critical review of microstructure and mechanical properties of laser welded similar and dissimilar titanium alloy joints. *Journal of Advanced Joining Processes*. 2024;9:100191. <https://doi.org/10.1016/j.jajp.2024.100191>
 28. Pawlik J, Cieřlik J, Bembenek M, Góral T, Kapayeva S, Kapkenova M. On the influence of linear energy/heat input coefficient on hardness and weld bead geometry in chromium-rich stringer GMAW coatings. *Materials*. 2022;15(17):6019. <https://doi.org/10.3390/ma15176019>
 29. Ou P, Cao Z, Hai M, Qiang J, Wang Y, Wang J, et al. Microstructure and mechanical properties of K-TIG welded dissimilar joints between TC4 and TA17 titanium alloys. *Materials Characterization*. 2023;196:112644. <https://doi.org/10.1016/j.matchar.2023.112644>
 30. Ranjan Giri S, Kumar Khamari B, Ranjan Moharana B. Joining of titanium and stainless steel by using different welding processes: A review. *Materials Today: Proceedings*. 2022;66:505–8. <https://doi.org/10.1016/j.matpr.2022.05.590>
 31. Niagaj J. Peculiarities of A-TIG welding of titanium and its alloys. *Archives of Metallurgy and Materials*. 2012;57. <https://doi.org/10.2478/v10172-011-0150-5>
 32. Kuppaswamy R, Calo K, Ramakumar J. Use of ResNet modelling for TIG weld feature digitization and correlation: a technique for AI based welding system. *Manufacturing Technology Today (MTT)*. 2023;22(1):25–32. <https://dx.doi.org/10.58368/mtt.22.1.2023.25-32>
 33. Guo Y, Chen F, Li M, Yu H, Li W, Deng H. The Effect of defect characteristics on prediction of fatigue life of TC4 titanium alloy welded joints. *Metals*. 2023;13(9):1540. <https://doi.org/10.3390/met13091540>
 34. Rogalski G, Świerczyńska A, Landowski M, Fydrych D. Mechanical and microstructural characterization of TIG welded dissimilar joints between 304L austenitic stainless steel and incoloy 800HT nickel alloy. *Metals*. 2020;10(5):559. <https://doi.org/10.3390/met10050559>
 35. Szwałka K, Zielińska-Szwałka J, Trzepieciński T. The influence of the shielding-gas flow rate on the mechanical properties of TIG-welded butt joints of commercially pure grade 1 titanium. *Materials*. 2024;17(5):1217. <https://doi.org/10.3390/ma17051217>

36. Minh PS, Nguyen V-T, Do TT, Uyen TMT, Song Toan HD, Linh HTT, et al. Parameter optimization in orbital TIG welding of SUS 304 stainless steel pipe. *Metals*. 2024;14(1):5. <https://doi.org/10.3390/met14010005>
37. Pan K, Hu H, Gu P. WD-YOLO: A more accurate YOLO for defect detection in weld x-ray images. *Sensors*. 2023;23(21):8677. <https://doi.org/10.3390/s23218677>
38. Liu T, Zheng P, Bao J. Deep learning-based welding image recognition: A comprehensive review. *Journal of Manufacturing Systems*. 2023;68:601–25. <https://doi.org/10.1016/j.jmsy.2023.05.026>
39. Zhang Y, Ni Q. A novel weld-seam defect detection algorithm based on the S-YOLO model. *Axioms*. 2023;12(7):697. <https://doi.org/10.3390/axioms12070697>
40. Kwon JE, Park JH, Kim JH, Lee YH, Cho SI. Context and scale-aware YOLO for welding defect detection. *NDT & E International*. 2023;139:102919. <https://doi.org/10.1016/j.ndteint.2023.102919>
41. Bembenek M, Prsyazhnyuk P, Shihab T, Machnik R, Ivanov O, Ropyak L. Microstructure and Wear characterization of the Fe-Mo-B-C—Based hard-facing alloys deposited by flux-cored arc welding. *Materials*. 2022;15(14):5074.
42. Zhang X, Zhao S, Wang M. Deep learning-based defects detection in keyhole TIG welding with enhanced vision. *Materials*. 2024;17(15):3871. <https://doi.org/10.3390/ma17153871>
43. Zhang S, Wang WY, Wang X, Li G, Ren Y, Gao X, et al. Large language models enabled intelligent microstructure optimization and defects classification of welded titanium alloys. *Journal of Materials Informatics*. 2024;4(4):34. <http://dx.doi.org/10.20517/jmi.2024.64>
44. ISO 15608:2017 – Welding – Guidelines for a metallic material grouping system. Geneva: ISO; 2017.
45. Winczek J, Gawronska E, Gucwa M, Szczygiol N. Theoretical and experimental investigation of temperature and phase transformation during SAW overlaying. *Applied Sciences*. 2019;9(7):1472. <https://doi.org/10.3390/app9071472>
46. Szala M, Walczak M, Hejwowski T. Factors influencing cavitation erosion of NiCrSiB hardfacings deposited by oxy-acetylene powder welding on grey cast iron. *Advances in Science and Technology Research Journal*. 2021;15(4):376–86. <https://dx.doi.org/10.12913/22998624/143304>
47. Kubiak M, Piekarska W, Saternus Z, Domański T. Numerical prediction of fusion zone and heat affected zone in hybrid Yb:YAG laser + GMAW welding process with experimental verification. *Procedia Engineering*. 2016;136:88–94. <https://doi.org/10.1016/j.proeng.2016.01.179>
48. Prsyazhnyuk P, Bembenek M, Drach I, Korzhov A, Romanyshyn L, Ropyak L. Restoration of the impact crusher rotor using FCAW with high-manganese steel reinforced by complex carbides. *Management Systems in Production Engineering*. 2024;32(2):294–302. <https://doi.org/10.2478/mspe-2024-0028>
49. Paszke AG, Sam Massa, F. PyTorch: An Imperative Style, High-Performance Deep Learning Library: Curran Associates, Inc.; 2019.
50. McKinney W. Data structures for statistical computing in python 2010;1–6.
51. Jocher GQ, Jing Chaurasia, Ayush Ultralytics YOLO.
52. PyTorch. AdamW – PyTorch documentation 2024 [Available from: <https://pytorch.org/docs/stable/generated/torch.optim.AdamW.html>].
53. Hunter JD. Matplotlib: A 2D graphics environment. *Computing in Science & Engineering*. 2007;9:90–5.